Cryogenic X-Ray Diffraction Microscopy for Biological Samples

Enju Lima,* Lutz Wiegart, Petra Pernot, Malcolm Howells, Joanna Timmins, Federico Zontone, and Anders Madsen†

European Synchrotron Radiation Facility, B.P. 220, F-38043 Grenoble, France

(Received 1 June 2009; revised manuscript received 14 August 2009; published 5 November 2009)

X-ray diffraction microscopy (XDM) is well suited for nondestructive, high-resolution biological imaging, especially for thick samples, with the high penetration power of x rays and without limitations imposed by a lens. We developed nonvacuum, cryogenic (cryo-) XDM with hard x rays at 8 keV and report the first frozen-hydrated imaging by XDM. By preserving samples in amorphous ice, the risk of artifacts associated with dehydration or chemical fixation is avoided, ensuring the imaging condition closest to their natural state. The reconstruction shows internal structures of intact *D. radiodurans* bacteria in their natural contrast.

DOI: 10.1103/PhysRevLett.103.198102 PACS numbers: 87.59.−e, 61.05.cp

In many aspects of science, seeing produces understanding. To advance our knowledge of the inner workings of cells it is important to be able to see what is there before us. Among the many advanced biological imaging methods there is currently no method that can image intact a-few-micron-thick samples in 3D, reaching the resolution of 10 nanometers (nm) or better, without the risk of structural artifacts. With such a method available, we may visualize the three-dimensional organization and interaction of subcellular organelles at the molecular level within an undisturbed, microns-size whole cell. The recently developed x-ray diffraction microscopy (XDM) has the potential to reach this goal [1–11]. The high penetration power of x rays allows probing thick samples without sectioning, while lens limitations, such as low efficiency or depth of focus, are no longer limiting factors to achieve high-resolution 3D imaging.

XDM has been demonstrated in the past in proof-of-principle experiments with test samples [1,2], nanocrystals to investigate strain field or core structures [3–5], biological samples [6–9], and deformation in a nanofoam [10]. The penetrating power of x rays allows XDM to probe thick samples that are not easily accessible by electron microscopy (EM), as demonstrated by x-ray microscopy based on Fresnel zone plates [12–15]. Thus, extensive sample preparation involving staining and sectioning, as well as cutting artifacts, can be avoided. By replacing a physical lens with a computational algorithm, one can, in principle, overcome optical limits and reach the maximum resolution given by the sample, i.e., the largest scattering angle measurable. By eliminating the poor efficiency and frequency response of the lens, the required radiation dose and the risk of radiation damage are reduced.

Previous biological XDM experiments have demonstrated its capabilities by imaging intact whole cells or subcellular organelles at 20–40 nm resolution [6–9]. So far, these experiments were conducted at room temperature with dried samples. Most biological samples are, however, highly aqueous and extremely sensitive to radiation damage. Therefore, in order to image them closest to their living state, frozen-hydrated imaging is necessary [16–19]. By rapidly freezing samples from the hydrated state into amorphous ice, one can capture the instantaneous morphology of the sample for imaging. Furthermore, ice at the cryogenic temperature immobilizes molecular fragments resulting from the initial ionizing radiation, thus further damage, such as mass loss, can be avoided. Towards 10 nm resolution, the radiation dose is expected to be above 10^8 Gray (Gy), causing unavoidable radiation damage on hydrated samples, unless they are cryoprotected [20–22].

We have developed nonvacuum cryo-XDM using hard x rays at 8 keV with a cryogenic gas-jet environment. By utilizing hard x rays, ''the thin sample approximation'' is valid for future 3D reconstructions through phasing a diffraction volume. Since a vacuum is not a requisite with hard x rays, the sample handling is facilitated with cryogenically cooled samples. Here, we report the first experimental demonstration of cryo-XDM for imaging intact, hydrated, and unstained biological samples. The 2D reconstruction of the frozen-hydrated *D. radiodurans* shows the cell's internal structures in natural contrast with a resolution of 30 to 50 nm.

XDM is an imaging method based on diffraction. When the diffracted wave field from a sample is known at the far field, the image reconstruction is straightforward by an inverse Fourier transformation. Experimentally, only the amplitude of the wave field is available as the phase is not measured. Sayre suggested that sampling the diffracted amplitude at the Nyquist frequency of the intensity pattern can encode phase information into the data [23]. Starting with such data, phase retrieval algorithms impose *a priori* known information as constraints iteratively to find a solution [24,25]. However, the convergence of the phasing algorithm is strongly dependent on the quality of the diffraction pattern. The general procedure outlined above has been used very successfully with radiation-hard samples, but obtaining quality data from weakly scattering biological samples, especially in the frozen state, has been challenging [26,27]. For successful imaging, one needs to

preserve the samples in the amorphous ice state throughout sample handling and data collection [17]. Otherwise, crystalline ice formation destroys fine structures in the sample and the diffraction signal is contaminated by strong ice-crystal scattering. The cryo-XDM developed here provides an efficient means of cryoprotection: by combining conventional plunge freezing of samples with data collection in the cryogenic-temperature gas environment, the risk of ice contamination is greatly reduced. The experimental details are summarized below.

D. radiodurans was chosen as a sample since its structure draws scientific interest in understanding radiation resistance and its size is suitable for XDM, but too thick for EM without sectioning [28]. The bacteria were cultured in TGY medium at 30 °C for 3 to 4 h in a shaking incubator, to select them during their exponential growth, and then dispersed into a water and glycerol solution (9:1 in volume) just before plunge freezing into liquid ethane. Glycerol was used as a cryoprotectant to ensure vitrification. Without the 10% glycerol, the plunge freezing usually produced crystalline ice, verified by powder diffraction patterns of the ice shown in Fig. 1(a). This is due to the ice thickness, ranging roughly from 5 to 10 μm which is too thick for a commercial plunge freezer to provide an efficient cooling rate. Replacing the plunge freezing with high pressure freezing would eliminate the need for the cryoprotectant in future experiments. The sample holders were commercially available nylon or kapton loops and the uniform water layer needed for XDM was obtained by surface tension without any supporting membrane. Before collecting coherent diffraction data, the ice quality was monitored by powder diffraction measurements to select vitrified samples as shown in Fig. 1(b). Figure 1(c) shows the schematic data collection setup for cryo-XDM. Since the absorption in air of 8 keV x rays is small, a nonvacuum environment is implemented for easy sample handling and monitoring by employing a macromolecular-crystallography-type sample environment [29]: samples are maintained in the vitrified state during data collection by bathing them in a continuous cryogenic nitrogen gas jet at around -165 °C, which isolates them from the surrounding warm air and prevents ice buildup. Sample positioning with respect to the beam and monitoring during data collection was done by a commercial on-axis visualization video microscope by MAATEL.

Coherent x-ray illumination on the sample is obtained by the combination of monochromator, mirrors, pinhole, and guard slits. After the silicon (111) monochromator and the higher-harmonics-rejecting mirrors, 8 keV x rays were spatially filtered by a 10 μm square pinhole to illuminate the samples coherently. In order to increase the photon flux at the sample, beryllium compound refractive lenses were used at 28 m upstream from the pinhole resulting in a flux of about 10^9 photons per second through the 10 μm pinhole. The unwanted airy pattern from the pinhole was blocked by secondary (guard) slits. Unfortunately, stray scattering from the guard slits was unavoidable and its effect on the diffraction data was noticeable when the samples were weakly scattering. The final diffraction data were collected on a charge-coupled device (CCD) with direct illumination and a pixel size of 22.5 μm, situated 2.2 m downstream of the sample.

Figure 2(a) shows a full diffraction pattern measured from frozen-hydrated, unstained *D. radiodurans*. The estimated radiation dose is $\sim 3 \times 10^7$ Gy and no signs of radiation damage were observed. As mentioned earlier, the scattering from the guard slits, shown as vertical and horizontal streaks, contaminated the data. To improve the convergence, the outer regions with streaks were masked out, but the contaminated central region could not be excluded since too much low-frequency data would be missing. To overcome this, a Butterworth-type high-pass filter was applied to the measured diffraction amplitude, $\sqrt{I}$, with the filter-cutoff frequency, f_{cutoff}, at 35 pixels [at $4 \times$ Nyquist frequency, where the Nyquist frequency is (sample dimension)$^{-1}$].

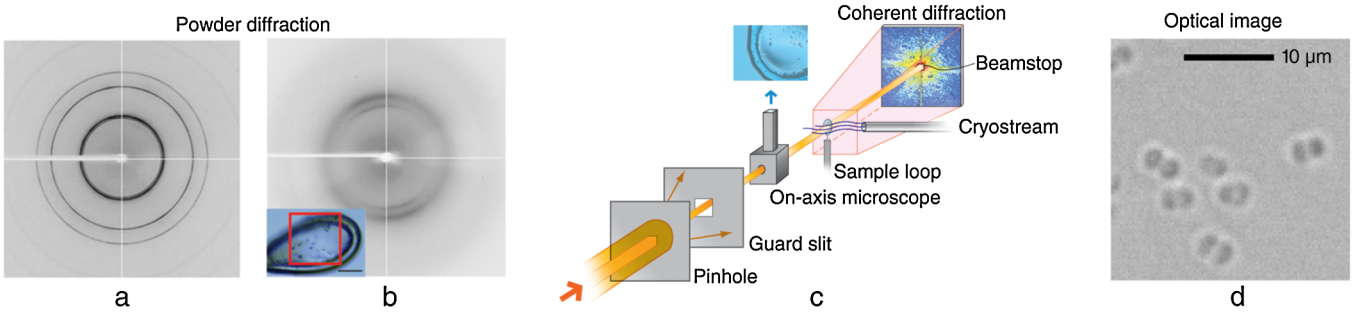

FIG. 1 (color online). (a) Characteristic powder diffraction pattern from crystalline (cubic) ice showing rings from (111), (220), and (311) planes corresponding to 3.666 , 2.248, and 1.891 Å d spacing, respectively. (b) Characteristic x-ray scattering of amorphous ice layer from a sample loop. The relatively sharp lines in the upper left and lower right resulted from scattering of the nylon loop, which was partially in the 100-μm-size beam (the square in the inset). (c) Experimental setup at ID10C, ESRF. The shaded region indicates a vacuum environment. The nonvacuum sample environment is a 40 cm long section of the beam path housing slits, a sample goniometer, an on-axis visualization video microscope by MAATEL, and an Oxford Cryostream cooler 700 series. (d) Optical microscope image of *D. radiodurans* with 320 $\times$ magnification.

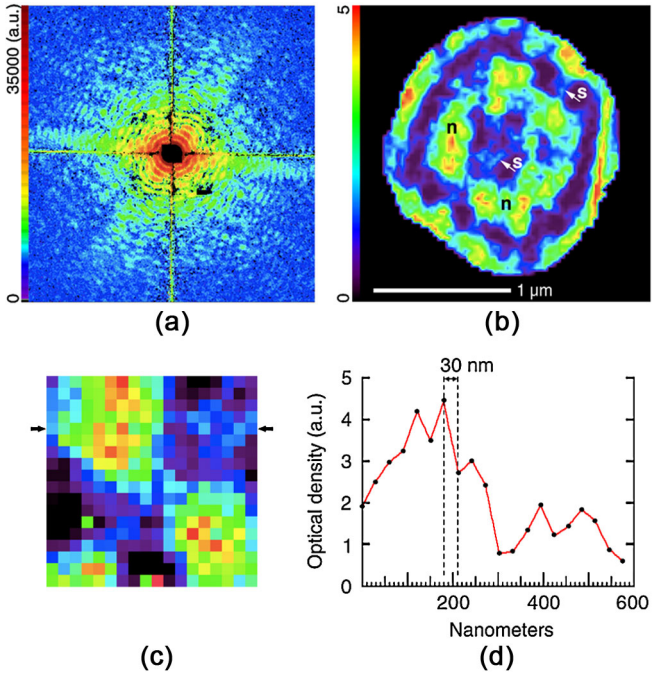

FIG. 2 (color online). (a) An assembled diffraction pattern of a frozen-hydrated *D. radiodurans*. The total exposure time is 7 min using focused 8 keV x rays. The measured diffraction signals at the edge of the array extend to 30 nm spatial half-period in the sample. (b) 2D reconstruction of *D. radiodurans*. The image is enlarged to a 210×210 pixel array from 70×70 pixel array using bilinear interpolation. The arrows at "*s*" highlight a diagonal structure which may be the septum and the areas labeled with "*n*" indicate possible nucleoid regions. (c) A zoomed-in region (the left middle section of 70×70 pixel array) which displays pixel resolution and features at 30 nm. (d) The image contrast along the 5th pixel row, indicated by arrows in (c).

$$(\sqrt{I})_{\text{filtered}} = \frac{1}{1 + \left(\frac{f_{\text{cutoff}}}{f}\right)^3} \sqrt{I}.$$

The phase retrieval of the diffraction pattern was carried out with the difference map with $\beta = 0.9$ [25]. A tight support was obtained by manually shrinking an initial support calculated from the autocorrelation of the sample. Since the support is manually adjusted, there is uncertainty of one or two pixels in the exact cell outline in some regions. The reconstruction shown at Fig. 2(b) was obtained by averaging the final reconstructions from 10 different random starts. The sample size is about 1.5 μm, calculated from the speckle size and reconstruction. Close observation suggests that the optically denser areas (labeled as "*n*") might be the nucleoid regions of the bacteria while "*s*" points out what may be the septa dividing the whole cell. However, the authors feel that this classification will require further studies into 3D reconstruction to avoid the ambiguity from the 2D projection of subcellular organelles. The future direction of the project will target a 3D reconstruction of a diffraction volume obtained by a tilt series on the sample.

The resolution in the current reconstruction is estimated to be 30 to 50 nm where features down to 30 nm are visible with a good contrast in Figs. 2(b)–2(d). The resolution measure based on the phase retrieval transfer function (PRTF [2,7,10]) shows the resolution cutoff frequency extends to the corner of the diffraction array at 20 μm^{-1} in Fig. 3, which corresponds to a 25 nm spatial half-period. We estimate that the PRTF provides the lower limit of the resolution (30 nm pixel resolution), while the contrast blur due to the 2D projection and the uncertainty of the cell boundaries place the upper limit of the resolution at 50 nm.

Any modification to the measured diffraction data needs to be studied carefully to ensure the validity of the reconstruction. In this effort, we have imaged a "known test sample" to evaluate the effect of the filtering process. Figure 4(a) shows a full diffraction pattern measured with 7.3 keV x rays from a 3-μm-size test sample made of tungsten. The SEM image is shown in (b). The two reconstructions, with and without the filter applied to the measured data, are shown in Figs. 4(c) and 4(d), which are almost identical. The comparison with the SEM image of the sample confirms the validity of the reconstructions with a pixel resolution of 25 nm [30]. We conclude that since most of the sample's structural information is carried in the phases of the diffraction pattern, the high-pass filtering of the diffraction amplitude, up to $4 \times$ Nyquist frequency, has no or minimal effect on the quality of reconstruction while it improves convergence of the phasing algorithm in the case of noisy data [31].

Experimental noise presents a challenging issue in XDM depending on the sample condition and may prevent convergence of the phasing algorithm. The current approach addresses a possible cause in the stagnation and demon-

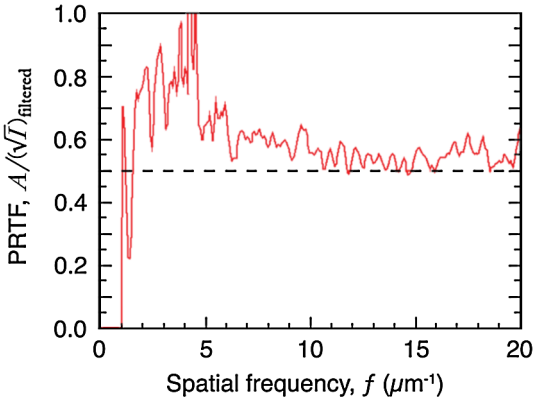

FIG. 3 (color online). The PRTF for the frozen-hydrated *D. radiodurans* reconstruction. $I(f)$ denotes the measured diffraction intensity and $A(f)$ is the Fourier amplitude from the reconstruction. Since the reconstruction was obtained after applying a high-pass filter to the diffraction data, the PRTF was calculated with $(\sqrt{I})_{\text{filtered}}$. The resolution cutoff frequency is determined where PRTF falls below 0.5 which extends to 20 μm^{-1} in the current reconstruction. The first dip down to 0.2 at the low frequency (near the beamstop edge) corresponds to the uncertainty in the exact cell boundaries.

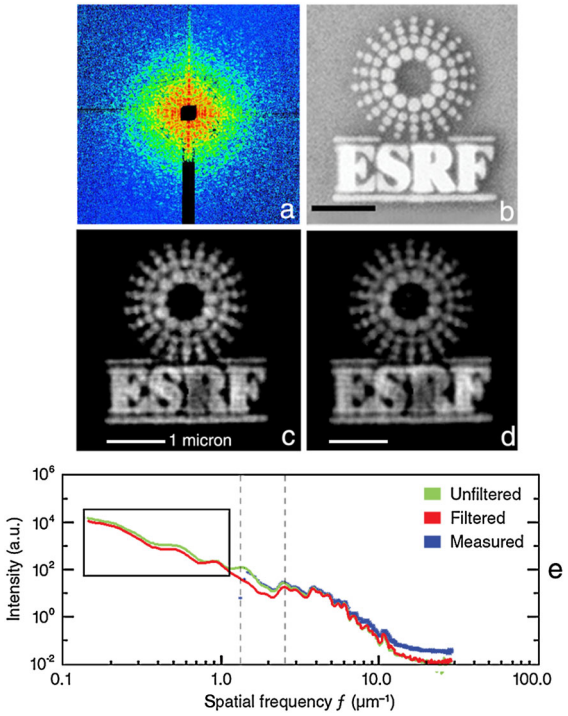

FIG. 4 (color online). (a) An assembled diffraction pattern, 540×540 pixel array, from a tungsten test sample measured with 7.3 keV x rays. (b) SEM image of the sample. (c) Reconstructions with high-pass-filtered diffraction amplitude with f_{cutoff} at 20 pixels (at $4 \times$ Nyquist frequency). (d) Reconstruction without high-pass filter. Bars indicate 1 μm. (e) Power spectrums of reconstructions (filtered, nonfiltered) and of measured data. The left dashed line indicates the start of the missing frequency and the right dashed line shows f_{cutoff}. By letting the missing data float during the iteration, the recovered Fourier amplitude, behind the beamstop (inset box), reached the same level of power density in both cases.

strates an efficient method to overcome the problem. We believe that extended data analysis to handle noisy data combined with an effort to improve the data quality will expand the scope of XDM to a wider range of samples.

In summary, we have reported the first frozen-hydrated imaging by XDM in an effort to image biological samples as close as possible to their natural state. In this first demonstration we have achieved a 30 to 50 nm resolution but we believe that the technique can be refined to achieve the radiation damage limit of 10 nm estimated by Howells *et al.* [22]. This estimation of the damage limit is based on the natural x-ray contrast between unmodified biological material and water. Resolution of less than 10 nm is expected to be within reach by the use of labeling and contrast-enhancing strategies or by use of short x-ray pulse ''diffraction-before-destruction'' [32] schemes.

We thank D. Guilligay at EMBL, Grenoble, G. Schoehn at IBS, Grenoble for their support during the sample preparation as well as M. Mattenet, E. Papillon, and the staff of ID10A/C at ESRF, for technical support at the beam line. We thank F. Glassmeier for help in the test sample imaging. The data analysis was supported in part by the U.S. Department of Energy under Contract No. DE-AC02-98CH10886.

*Corresponding author.
elima@bnl.gov
Present address: Brookhaven National Laboratory, Upton, NY 11973, USA.
†amadsen@esrf.fr

[1] J. Miao, P. Charalambous, J. Kirz, and D. Sayre, Nature (London) **400**, 342 (1999).
[2] H. N. Chapman *et al.*, J. Opt. Soc. Am. A **23**, 1179 (2006).
[3] G. J. Williams, M. A. Pfeifer, I. A. Vartanyants, and I. K. Robinson, Phys. Rev. Lett. **90**, 175501 (2003).
[4] J. Miao *et al.*, Phys. Rev. Lett. **97**, 215503 (2006).
[5] M. A. Pfeifer *et al.*, Nature (London) **442**, 63 (2006).
[6] J. Miao *et al.*, Proc. Natl. Acad. Sci. U.S.A. **100**, 110 (2003).
[7] D. Shapiro *et al.*, Proc. Natl. Acad. Sci. U.S.A. **102**, 15343 (2005).
[8] C. Song *et al.*, Phys. Rev. Lett. **101**, 158101 (2008).
[9] Y. Nishino, Y. Takahashi, N. Imamoto, T. Ishikawa, and K. Maeshima, Phys. Rev. Lett. **102**, 018101 (2009).
[10] A. Barty *et al.*, Phys. Rev. Lett. **101**, 055501 (2008).
[11] C. G. Schroer *et al.*, Phys. Rev. Lett. **101**, 090801 (2008).
[12] J. Kirz, C. Jacobsen, and M. Howells, Q. Rev. Biophys. **28**, 33 (1995).
[13] Y. Wang, C. Jacobsen, J. Maser, and A. Osanna, J. Microsc. **197**, 80 (2000).
[14] D. Weiss *et al.*, Ultramicroscopy **84**, 185 (2000).
[15] C. A. Larabell and M. A. Le Gros, Mol. Biol. Cell **15**, 957 (2004).
[16] R. M. Glaeser and K. A. Taylor, J. Microsc. **112**, 127 (1978).
[17] J. Dubochet *et al.*, *Cryotechniques in Biological Electron Microscopy*, edited by R. A. Steinbrecht and K. Zierold (Springer-Verlag, Berlin, 1987), pp. 114–131.
[18] G. Schneider, Ultramicroscopy **75**, 85 (1998).
[19] J. Maser *et al.*, J. Microsc. **197**, 68 (2000).
[20] S. Williams *et al.*, J. Microsc. **170**, 155 (1993).
[21] Q. Shen, I. Bazarov, and P. Thibault, J. Synchrotron Radiat. **11**, 432 (2004).
[22] M. Howells *et al.*, J. Electron Spectrosc. Relat. Phenom. **170**, 4 (2009).
[23] D. Sayre, Acta Crystallogr. **5**, 843 (1952).
[24] J. R. Fienup, Appl. Opt. **21**, 2758 (1982).
[25] V. Elser, J. Opt. Soc. Am. A **20**, 40 (2003).
[26] E. Lima, Ph.D thesis, Stony Brook University, 2006.
[27] D. Sayre, Acta Crystallogr. Sect. A **64**, 33 (2008).
[28] A. W. Anderson *et al.*, Food Technol. **10**, 575 (1956).
[29] E. F. Garman and T. R. Schneider, J. Appl. Crystallogr. **30**, 211 (1997).
[30] The PRTFs obtained in both cases show the resolution cutoff frequency extending to the corner of the measured diffraction pattern at 25 μm^{-1}.
[31] The further study on the effect of the filtering as a function of f_{cutoff} shows high-pass filtering can be applied to 7 to $8 \times$ Nyquist frequency with moderate edge-enhancement effect in the image.
[32] H. N. Chapman *et al.*, Nature Phys. **2**, 839 (2006).